

Mammalian Complex I Pumps 4 Protons per 2 Electrons at High and Physiological Proton Motive Force in Living Cells*

Received for publication, December 10, 2012, and in revised form, January 9, 2013. Published, JBC Papers in Press, January 10, 2013, DOI 10.1074/jbc.M112.438945

Maureen O. Ripple, Namjoon Kim, and Roger Springett¹

From the Department of Radiology, Geisel School of Medicine at Dartmouth, Hanover, New Hampshire 03755

Background: The $H^+/2e^-$ stoichiometry of complex I has been questioned based on recent crystal structures.

Results: A new method of quantitating proton motive force and ubiquinone redox potential was used to determine the thermodynamic poise of complex I in living cells.

Conclusion: The poise is consistent with pumping 4 not $3H^+/2e^-$.

Significance: This new methodology can quantitate electron transport chain function in living cells.

Mitochondrial complex I couples electron transfer between matrix NADH and inner-membrane ubiquinone to the pumping of protons against a proton motive force. The accepted proton pumping stoichiometry was 4 protons per 2 electrons transferred ($4H^+/2e^-$) but it has been suggested that stoichiometry may be $3H^+/2e^-$ based on the identification of only 3 proton pumping units in the crystal structure and a revision of the previous experimental data. Measurement of proton pumping stoichiometry is challenging because, even in isolated mitochondria, it is difficult to measure the proton motive force while simultaneously measuring the redox potentials of the NADH/NAD⁺ and ubiquinol/ubiquinone pools. Here we employ a new method to quantify the proton motive force in living cells from the redox poise of the *bc₁* complex measured using multiwavelength cell spectroscopy and show that the correct stoichiometry for complex I is $4H^+/2e^-$ in mouse and human cells at high and physiological proton motive force.

Mitochondrial complex I is a transmembrane protein containing 45 subunits (980 kDa) that oxidizes matrix NADH to NAD⁺, reduces membrane-bound ubiquinone (UQ)² to ubiquinol (UQH₂) and pumps protons across the inner mitochondrial membrane against a proton motive force (ΔP) (1). Although crystal structures of the mammalian complex are not available, recent structures of the prokaryotic complex, which contain the 14 core subunits (580 kDa) that are conserved from bacteria to humans (2), and the eukaryote complex from *Yarrowia lipolytica* have shown that the electron transfer pathway is contained in a hydrophilic domain that extends into the matrix and is physically separated from the membrane domain

where the proton pumping is believed to occur (2–3). The mechanism by which electron transfer is coupled to proton pumping is not known but most models assume that electron transfer in the hydrophilic domain is coupled to a conformational change in the membrane domain.

The membrane domain contains three subunits ND2, ND4, and ND5, which are both homologous to each other and to the Na⁺/H⁺ exchanger (2, 4) and are likely the proton pumping units. These domains abut each other and are coupled together by a helix that runs parallel to the membrane suggesting that it acts to synchronize the conformational change in all three subunits (5–6). Previous studies have concluded that complex I pumps 4 protons per 2 electrons transferred ($4H^+/2e^-$) (7) but the observation that there are only 3 proton pumping units has prompted a re-evaluation of the data suggesting a stoichiometry of $3H^+/2e^-$ (8). Here we show that the correct stoichiometry is $4H^+/2e^-$ when complex I operates in the mitochondria of living cells.

The proton pumping stoichiometries of the electron transport chain complexes (H^+/e^- ratios) and the stoichiometry of ATP production to electron transport (P/O ratios) can be measured either functionally or thermodynamically. Both methods require the complex to be integrated into a membrane either in mitochondria, submitochondrial particles, or proteoliposomes. The former method measures the stoichiometry from the quantity of protons extruded (H^+/e^-) or the ATP-generated (P/O) for a given quantity of electrons transferred (9). Accuracy requires the minimization of proton leak so that the measurement is usually carried out in the absence of ΔP . A complication is that the proton pumping being measured can generate a ΔP , which subsequently drives the proton leak (10). It is also difficult to separate the contribution of complex I from that of the *bc₁* complex so that the stoichiometry of complex I is usually measured from the difference of complex I+III, measured with a complex I substrate such as malate/glutamate or β -hydroxybutyrate, and complex III, measured using the complex II substrate, succinate.

The thermodynamic method of measuring the H^+/e^- ratios and the P/O ratios is based on the ATP phosphorylation potential achieving equilibrium with the electron transport chain from NADH to cytochrome *c* when the electron flux is zero (11). Equilibrium of the overall reaction requires equilibrium of

* This work was supported, in whole or in part, by Grants 5R21RR25803 and R01NS054298 from the National Institutes of Health.

¹ To whom correspondence should be addressed: Remsen 319, Department of Radiology, Geisel School of Medicine at Dartmouth, Hanover, NH 03755. Tel.: 603-650-1625; E-mail: RSpringett@Dartmouth.edu.

² The abbreviations used are: UQ, ubiquinone; $\Delta\Psi$, mitochondrial membrane potential; ΔpH , pH gradient; ΔP , proton motive force expressed in millivolts; UQH₂, ubiquinol; E_{i-UQ} , redox potential of the membrane UQH₂/UQ pool; E_{i-NADH} , redox potential of the matrix NADH/NAD⁺ pool; Cyt_c, cytochrome *c*; CytOx, cytochrome oxidase; ΔE_s , redox span of complex I; n_p , proton pumping stoichiometry of complex I; VO₂, oxygen consumption; 3-NPA, 3-nitropropionic acid; CCCP, carbonyl cyanide *m*-chlorophenyl hydrazone.

the partial reactions so that both complex I and the bc_1 complex must operate at equilibrium with ΔP when electron flux is zero. In this case, the energy released on electron transfer between substrate and product redox pools is equal to the energy required to pump the protons. For complex I, this relates the difference in redox potentials of the UQH_2/UQ and NADH/NAD^+ pools (the redox span, ΔE_s) to the product of the proton pumping stoichiometry and ΔP . This method is complicated by the difficulty in simultaneously and precisely measuring the redox poise of the NADH/NAD^+ and UQH_2/UQ pools and in quantitating ΔP . Often ΔP is estimated from the phosphorylation potential assuming an ATP/H^+ stoichiometry, which was previously thought to be 3 (7) but has now been revised to 8/3 based on the crystal structure of the ATP synthase (12).

Recently we have developed a methodology to calculate the membrane potential ($\Delta\Psi$) and pH gradient (ΔpH) components of ΔP as well as the redox potential of the UQH_2/UQ pool from the redox poise of the bc_1 complex measured using multiwavelength cell spectroscopy in living cells (13). Combined with NADH fluorescence spectroscopy to measure the oxidation state of mitochondrial NADH, it provides all the necessary parameters to examine the thermodynamic poise of complex I in mitochondria respiring in the authentic environment of a living cell. We find that the thermodynamic poise is consistent with pumping $4\text{H}^+/2\text{e}^-$ both at high ΔP and under physiological conditions in mouse and human cells.

EXPERIMENTAL PROCEDURES

Cell Culture—RAW 264.7 mouse macrophage cells and human leukemia HL-60 cells were cultured at 37°C in spinner flasks in phenol-red free RPMI medium (Invitrogen) containing antibiotic/antimycotic (Sigma) and 10% fetal bovine serum (Invitrogen) in a 95% air and 5% CO_2 incubator.

Cell Oxygenation and Oxygen Consumption—Cells were spun down at $500 \times g$ for 5 min and then resuspended at a density of 2.0×10^7 cells/ml in RPMI medium and placed in a custom-built 5 ml chamber that consisted of a 17 mm inside-diameter quartz crucible embedded in an aluminum block maintained at 37.0°C by a thermoelectric element. The oxygen concentration within the chamber was measured from the fluorescence lifetime of a phosphorescent membrane inserted through a 3-mm diameter hole in the side of the crucible and the top of the chamber was sealed with a stainless steel plunger. The stir bar was made of glass rather than Teflon, and all the seals were made of viton in accordance with good respirometry practice (14). The cells were oxygenated and deoxygenated under computer control by exchange of oxygen across 80 mm of oxygen-permeable silicone tubing immersed in the cell suspension using a feedback circuit to adjust the oxygen tension within the tubing to maintain constant oxygenation within the chamber; the tubing always contained 5% CO_2 to maintain intracellular pH. Oxygen consumption was measured from the difference between the oxygen delivery to the cell suspension by the tubing and the rate change of the oxygen concentration of the cell suspension. The oxygen delivery was calculated from the oxygen gradient across the wall of tubing and the oxygen-permeability of the tubing, which was measured prior to each study.

Spectroscopy and Spectral Analysis—The spectroscopy system has been described previously (13). In brief, heme attenuation spectra and NADH fluorescence spectra were measured with two separate CCD-spectrograph systems working in time-multiplexed mode at 50 Hz, and contiguous spectra were averaged to give a temporal resolution of 0.5 s. A warm white light emitting diode (LED) was used for the attenuation spectra illumination, and a 365 nm UV LED was used for NADH fluorescence excitation.

The spectral fitting algorithms employed a linear combination of model spectra to calculate oxidation changes of the hemes and NADH as described previously (13). For heme oxidation changes, the model spectra were b_H , b_L , c_1 hemes of the bc_1 complex, heme c of cytochrome c , a_{605} , a_{602} , and a_3 spectra from cytochrome oxidase (15) and a quadratic background to account for any baseline drift with a fitting range 520–630 nm. The oxidized fraction of each heme (oxidation state) was calculated from the oxidation changes assuming full reduction during anoxia and full oxidation at high oxygen tension after addition of $1 \mu\text{M}$ of the complex I inhibitor rotenone.

The NADH model spectra were the fluorescence spectrum of NADH, the fluorescence spectrum of the RPMI medium, and a linear background with a fitting range of 419–610 nm. The NADH signal originates from both NADH and NADPH in both the cytosol and the mitochondria. The oxidation state of mitochondrial NADH was calculated from oxidation changes assuming full reduction of mitochondrial NADH during anoxia and full oxidation of mitochondrial NADH after 1 mM of the complex II inhibitor 3-nitropropionic acid (3-NPA), which inhibits the TCA cycle, and $1 \mu\text{M}$ protonophore carbonyl cyanide *m*-chlorophenyl hydrazone (CCCP) assuming that NADPH and cytosolic NADH did not change with these interventions.

Measurement of ΔP and Redox Potentials—The redox potential of the UQH_2/UQ pool, $\Delta\Psi$ and ΔpH were measured from the redox poise of the bc_1 complex as described previously (13) and shown graphically in Fig. 1 where the redox potential is plotted on the y axis and the bell-shaped curves are a precise graphical representation of the Nernst equation, with the gray area representing the reduced fraction, the white area representing the oxidized fraction, and the line of symmetry is the midpoint potential. The redox plot of the UQH_2/UQ couple is narrower than the hemes because it is an $n = 2$ electron carrier. In brief, the oxidation state of b_H and b_L of the bc_1 complex and the oxidation state of Cyt c was measured with multiwavelength cell spectroscopy. Redox potentials were then calculated from the oxidation states using the Nernst equation ($n = 1$) for Cyt c and a model of redox anti-cooperativity for b_H and b_L . $\Delta\Psi$ was calculated from the redox poise of the b_H and b_L hemes assuming the centers are in redox equilibrium and separated by $1/2$ the membrane dielectric. The redox potential of the UQH_2/UQ pool was calculated from the redox potential of b_H assuming equilibrium and that the b_H center is located at a distance of $1/4$ membrane dielectric into the membrane. Finally, ΔpH was calculated from the redox span of the bc_1 complex correcting for the disequilibrium ($-\Delta G^{\text{III}}$) of the bc_1 complex using a stochastic model of turnover. ΔP is the sum of $\Delta\Psi$ and ΔpH when ΔpH is expressed in millivolts.

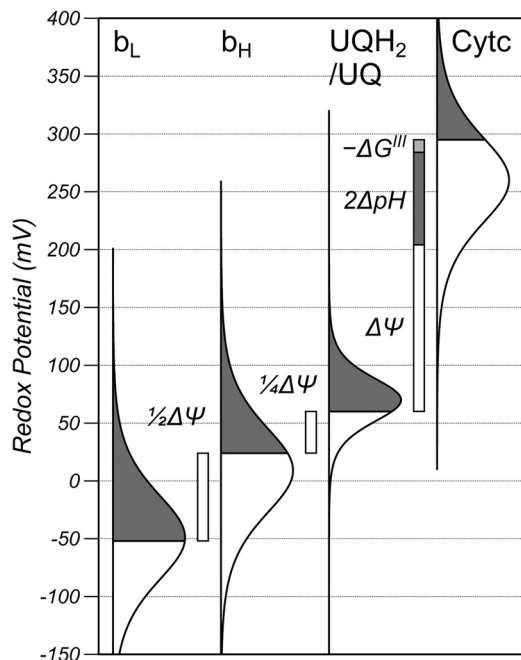
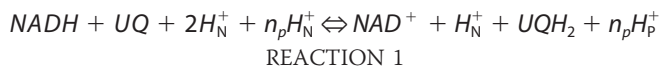


FIGURE 1. The redox poise of the bc_1 complex in RAW cells under normal conditions and relationship between the redox potentials, $\Delta\Psi$, ΔpH , and the disequilibrium of the bc_1 complex ($-\Delta G'''$). The redox potential is plotted on the y axis, and the bell-shaped curves are a precise graphical representation of the Nernst equation, where the gray area represents the reduced fraction, the white area represents the oxidized fraction, and the line of symmetry is the midpoint potential. The shape of the UQH_2/UQ curve is narrower than the hemes because it is an $n = 2$ electron carrier, and the midpoint has been shifted from the pH 7.0 value (90 mV) to account for the pH of the matrix. The b_H and b_L curves are shown as simple $n = 1$ Nernst functions with effective midpoint potentials of 9 and -49 mV, respectively, to account for their oxidation state, but the actual shapes are more complicated because of their redox anti-cooperativity.

The redox potential of the $NADH/NAD^+$ pool was calculated from the oxidation state of $NADH$ measured with fluorescence spectroscopy using the Nernst equation ($n = 2$) and a pH-dependent midpoint potential of -320 mV + 30.75 mV/pH unit at 37°C . The pH of the matrix was calculated from ΔpH assuming the cytosol remained at pH 7.0.

Thermodynamic Analysis—Complex I catalyzes Reaction 1,



where H_N^+ and H_P^+ are protons on the negative (matrix) and positive (cytosolic) side of the membrane, respectively, and n_p is the number of protons pumped per two electrons transferred. The Gibbs free energy for this reaction is given by Equation 1,

$$\Delta G = -2(E_h^{UQ} - E_h^{NADH}) + n_p \Delta P \quad (\text{Eq. 1})$$

where E_h^{UQ} and E_h^{NADH} are the redox potentials of the UQH_2/UQ and $NADH/NAD^+$ pools with respect to proton concentration in the matrix, respectively. The term in brackets is the redox span of complex I (ΔE_s), and is the free energy released when an electron is passed from the $NADH/NAD^+$ pool to the UQH_2/UQ pool; the factor of 2 accounts for the 2-electron transfer. The second term on the right is the free energy required to pump the protons. ΔG is zero when the enzyme operates at equilibrium and the flux is zero. A disequi-

librium between substrate and products drives a net flux such that ΔG is negative when the enzyme operates in the forward direction, and ΔG is positive when it operates in the reverse direction.

As ΔG is always smaller or equal to zero for normal turnover, and ΔP is always positive, Equation 1 can be expressed as $2\Delta E_s/\Delta P \geq n_p$, where the equality holds at equilibrium (zero flux) and the inequality at net forward flux. It is not possible to poise the electron transport chain at intermediate redox potentials at zero flux in living cells so the approach in this report is to measure $2\Delta E_s/\Delta P$ at varying flux from low to intermediate values and then extrapolate back to zero flux where ΔG is zero and the equality holds.

Unlike the bc_1 complex, the electron flux through complex I cannot be calculated from the mitochondrial oxygen consumption because the content of complex I is not known and because the electron flux to oxygen may include electron flux through complex II and through acyl-CoA dehydrogenase because of the oxidation of succinate and β -oxidation of fatty acids, respectively. The electron flux through the bc_1 complex can be used as an index of the electron flux through complex I, because the stoichiometry of complex I to complex III is constant over the short period of these studies and the two fluxes are likely to be proportional.

The thermodynamic efficiency (ϵ) is the fraction of the energy released on electron transfer that is transduced into the proton motive force and given by $\epsilon = n_p \Delta P / 2\Delta E_s$.

RESULTS

Fig. 2 shows an example of the measurement protocol. Cells were placed in the chamber and the oxygenation maintained at $100 \mu\text{M}$ at all times except during the shaded area when the oxygen tension was reduced to zero for 2 min under computer control to fully reduce the electron transport chain hemes and mitochondrial $NADH$ before being returned to $100 \mu\text{M}$. The cells were then treated with $6 \mu\text{M}$ oligomycin (arrow O), an ATP synthase inhibitor, to decrease proton influx into the matrix and decrease oxygen consumption. The cells were then treated with 5 doses of 50 nM CCCP (arrows C) to increase proton leak through the inner mitochondrial membrane and stimulate oxygen consumption in small increments. This was followed by $1 \mu\text{M}$ CCCP (arrow U) and 1 mM of 3-NPA (arrow N) to fully oxidize the mitochondrial pool of $NADH$ and then $1 \mu\text{M}$ of the complex I inhibitor rotenone (arrow R) to fully oxidize the hemes. The spikes in the oxygen consumption (VO_2) trace on addition of drugs are artifacts resulting from the small quantity of oxygen dissolved in the solvent. The lower panel of Fig. 2 shows the calculated ΔP , $\Delta\Psi$, and ΔpH (expressed in millivolts where $1\text{pH unit} \approx 61.5$ mV at 37°C) for this dataset obtained from averages of 30 s of data from the baseline period, after oligomycin and after the 5 additions of CCCP. Oligomycin resulted in increases in $\Delta\Psi$ and ΔpH as expected and addition of CCCP in 50 nM steps decreases $\Delta\Psi$ while ΔpH remained approximately constant. In contrast to $NADH/NAD^+$, which undergoes a substantial reduction, the redox potential of UQH_2/UQ barely changes on addition of oligomycin but both $NADH/NAD^+$ and the UQH_2/UQ pools oxidize on addition of CCCP.

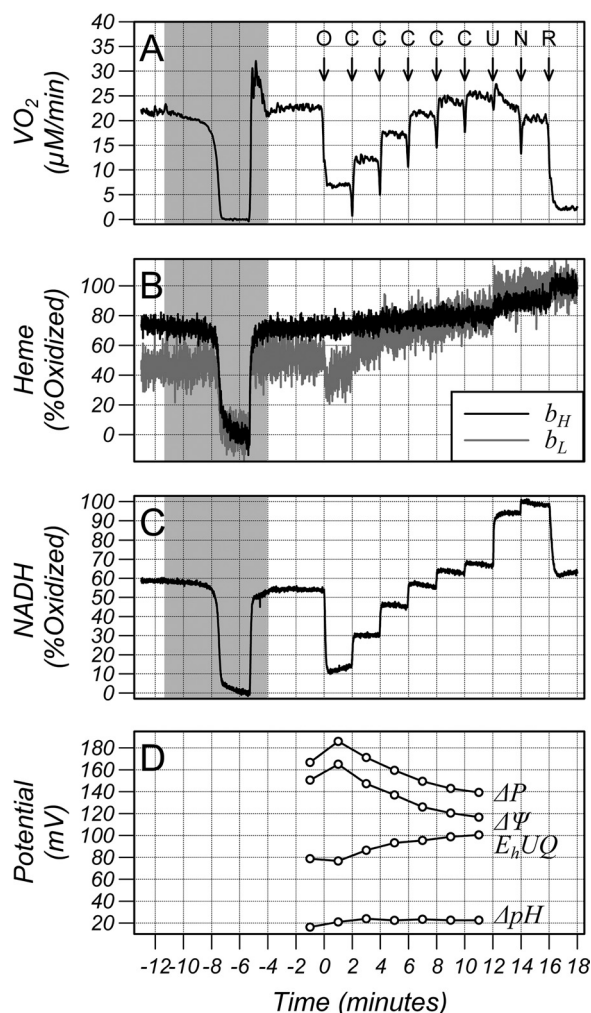


FIGURE 2. Traces from a typical study in HL-60 cells of (A) oxygen consumption (VO_2), (B) oxidation state of the b_H and b_L hemes of the bc_1 complex, (C) oxidation state of NADH/NAD⁺, and (D) membrane potential ($\Delta\Psi$), pH gradient (ΔpH), proton motive force (ΔP), and redox potential of the UQH₂/UQ pool (E_h UQ) calculated from an average over 30 s. A downward deflection denotes reduction. The pH gradient is expressed in millivolts where 1 pH unit = 61.5 mV at 37 °C. The oxygen concentration was maintained at 100 μM at all times except during the shaded area when the oxygen tension was reduced to zero for 2 min under computer control and then returned to 100 μM . Additions to the chamber were marked with arrows, O: 5 $\mu g/ml$ oligomycin, C: 50 nM CCCP, U: 1 μM CCCP, N: 1 mM 3-NPA, and R: 1 μM rotenone. The spikes in the oxygen consumption (VO_2) trace on addition of drugs are artifacts resulting from the small quantity of oxygen dissolved in the solvent.

The proton pumping stoichiometry of complex I is equal to $2\Delta E_s/\Delta P$ when the enzyme is at equilibrium and $<2\Delta E_s/\Delta P$ when the disequilibrium generates a net electron flux. The relationship between bc_1 electron flux, which is used as an index of complex I electron flux, and ΔP , ΔE_s , and $2\Delta E_s/\Delta P$ is shown in Fig. 3 for HL-60 and RAW cells for the oligomycin-inhibited state (lowest electron flux) and three additions of CCCP (50 nM for the HL-60 cells and 200 nM for the RAW cells). The parameters are approximately linear with respect to electron flux and so can be extrapolated to zero flux to determine the values that they would have if complex I were working at equilibrium and when $2\Delta E_s/\Delta P$ is equal to proton pumping stoichiometry. Values were extrapolated by performing a linear regression using the data of each individual study resulting in values of $197 \pm$

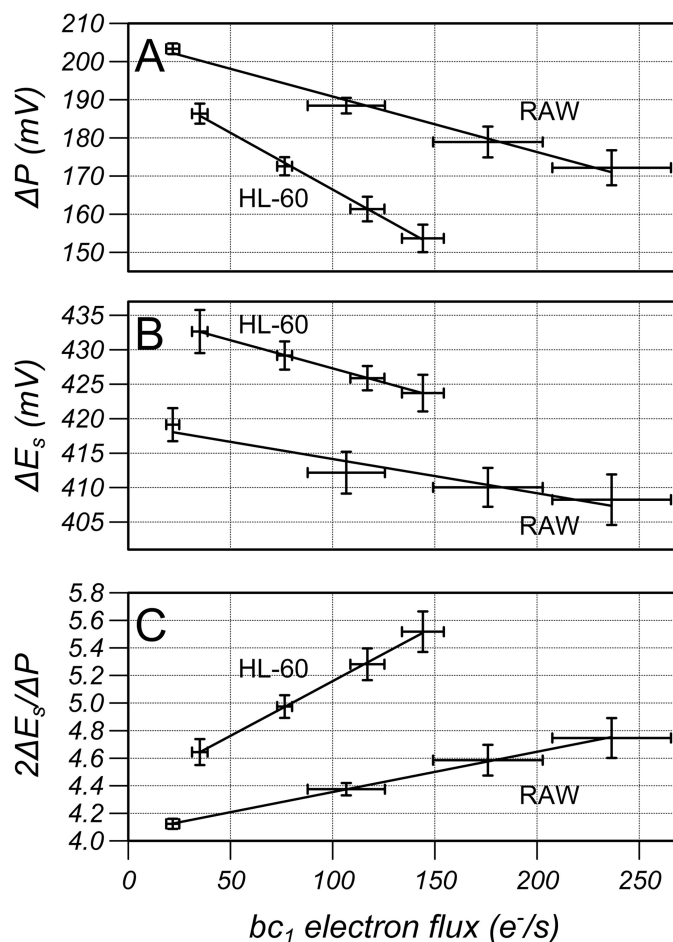


FIGURE 3. The relationship between bc_1 electron flux measured in electrons per second per enzyme and (A) proton motive force (ΔP), (B) redox span (ΔE_s), and (C) $2\Delta E_s/\Delta P$ for RAW and HL-60 cells from the oligomycin-inhibited state (lowest bc_1 electron flux) and 3 additions of CCCP. $2\Delta E_s/\Delta P$ is equal to the proton pumping stoichiometry when the electron flux is zero. Results are mean \pm S.D. ($n = 6$) with a linear regression line to the mean data.

3mV, $435 \pm 3mV$ and 4.4 ± 0.1 for ΔP , ΔE_s , and $2\Delta E_s/\Delta P$ for HL-60 cells, respectively, and $205 \pm 1mV$, $419 \pm 2mV$ and 4.1 ± 0.1 for RAW cells, respectively (mean \pm S.D., $n = 6$).

An alternative method to vary electron flux of RAW cells is to culture them overnight in glutamine-free media and then restore glutamine in the measurement chamber. This represents a purely physiological method of varying electron flux. This cannot be done in HL-60 cells because they rapidly lose their viability when cultured in the absence of glutamine whereas RAW cells maintain their viability greater than 97% after 2 days cultured in the absence of glutamine. RAW cells cultured in glutamine containing media had a baseline bc_1 electron flux of $155 \pm 11e^-/s$ (mean \pm S.D., $n = 6$). This decreased to $94 \pm 8e^-/s$ when cells were cultured in the absence of glutamine and then almost doubled to $161 \pm 12e^-/s$ 15 min after addition of 2 mM glutamine. Fig. 4 shows ΔP , ΔE_s , and $2\Delta E_s/\Delta P$ as a function of bc_1 turnover measured prior to addition of glutamine and then every 2 min after addition of glutamine and these terms were found to be approximately linear with bc_1 turnover under these conditions. Extrapolating the dependence back to zero flux yields $195 \pm 2mV$, $393 \pm 2mV$, and 4.0 ± 0.1 for ΔP , ΔE_s , and $2\Delta E_s/\Delta P$, respectively (mean \pm S.D., $n = 6$).

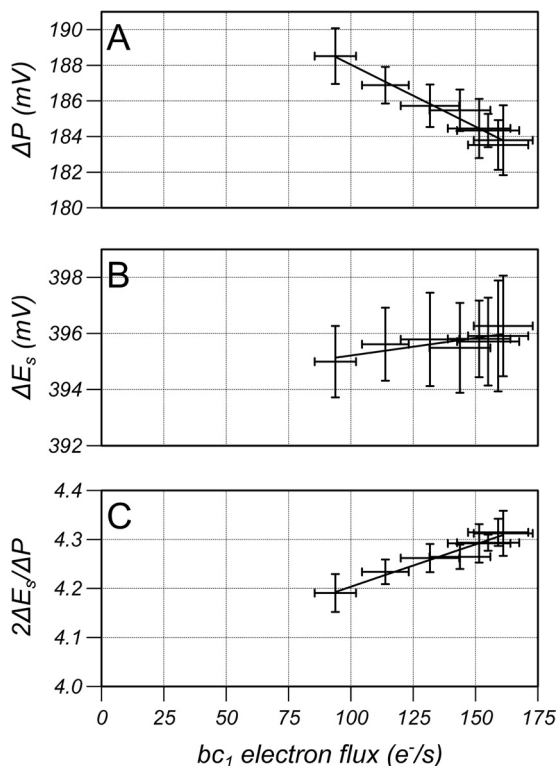


FIGURE 4. The relationship between bc_1 electron flux measured in electrons per second per enzyme and (A) proton motive force (ΔP), (B) redox span (ΔE_s), and (C) $2\Delta E_s/\Delta P$ for RAW cells without glutamine (lowest bc_1 electron flux) and every 2 min after addition of 2 mM glutamine. $2\Delta E_s/\Delta P$ is equal to the proton pumping stoichiometry when the electron flux is zero. Results are mean \pm S.D. ($n = 6$) with a linear regression line to the mean data.

The bc_1 turnover as a function of ΔG and thermodynamic efficiency is shown in Fig. 5 for the data from Figs. 3 and 4 assuming a proton pumping stoichiometry of $4H^+/2e^-$. The disequilibrium ($\Delta G < 0$) drives electron flux but greater changes in ΔG were required to drive the same flux (measured through the bc_1 complex) in HL-60 cells compared with RAW cells when flux was increased with CCCP from the oligomycin-inhibited state, and smaller changes in ΔG were required when flux was increased by the addition of glutamine. This is reflected in Fig. 5B as a lower thermodynamic efficiency, that is, for a given electron flux, a lower fraction of energy released on electron transfer from the NADH/NAD⁺ to the UQH₂/UQ pools was transduced into the proton motive force and made available for ATP synthesis. In the absence of inhibitors, complex I operated at an efficiency of $>92\%$ in RAW cells.

DISCUSSION

In this report, a new methodology was employed to calculate ΔP across the inner membrane of mitochondria in living cells from the redox poise of the bc_1 complex and used to estimate the thermodynamic poise of complex I. The b_H and b_L hemes straddle the membrane and form an intrinsic sensor of the potential difference between them due to the electric field generated by $\Delta\Psi$. The forward and reverse rate constants for electron transfer, based on the Dutton Ruler (16), are $\approx 10^6$ and 10^5 per second, which is much faster than net flux of $\approx 10^2$ per second (Fig. 5) ensuring that they remain in close equilibrium as confirmed by a full kinetic model of the bc_1 complex in the

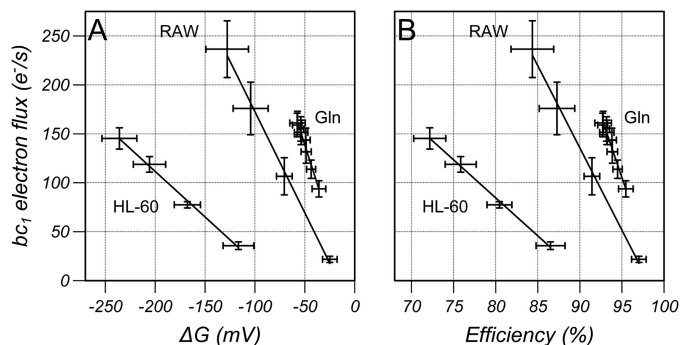


FIGURE 5. The bc_1 electron flux plotted as a function of (A) ΔG and (B) thermodynamic efficiency calculated assuming a proton pumping stoichiometry of $4H^+/2e^-$ for the data from Figs. 2 (RAW and HL-60) and 3 (Gln). Results are mean \pm S.D. ($n = 6$) with a linear regression line to the mean data.

presence of ΔP (13). Once equilibrium is assumed, the difference in the redox potentials of the hemes is then equal to $\beta\Delta\Psi$, where β is the fractional dielectric separation of the hemes, which has been measured to be 0.5 (17).

The hemes are embedded in the Cytb subunit, which defines the intermediate dielectric constant rather than the membrane whose lipid composition could be variable. The calculation of $\Delta\Psi$ then requires conversion of the oxidation states to redox potentials using the midpoint potentials and anticooperative interaction determined previously (17). This is a more direct method of quantifying the membrane potential than using fluorescence microscopy to measure the accumulation of a cationic membrane-permeable fluorescent probe and involves fewer assumptions, see Gerencser *et al.* (18). The redox potential of the membrane-bound UQH₂/UQ pool is calculated assuming equilibrium with b_H through the Qi center and that b_H is at a dielectric distance of 0.25 from the matrix. The dielectric distance was estimated from the crystal structure. A 20% error (a dielectric distance of 0.2 or 0.3) would lead to an 8 mV error in the redox potential of the UQH₂/UQ pool and a 3% error in the estimation of the proton pumping stoichiometry. The forward and reverse binding rates of UQ and UQH₂ at the Qi center are 10^5 to 10^8 per second assuming a UQ concentration of 30 mM in the membrane, and the electron transfer rates are of the order of 10^5 - 10^9 per second (19); both values are much faster than the net flux. The kinetic model predicted a maximum disequilibrium of 8mV (producing a 3% error in the proton pumping stoichiometry) when the bc_1 complex operated at low $\Delta\Psi$ and the UQ/UQH₂ ratio was 9.5 (13), conditions not found in this study.

The pH gradient is calculated from the redox span of UQH₂ to Cytc, and, in this case, redox equilibrium cannot be assumed and must be estimated from the redox poise and flux of the bc_1 complex using the kinetic model. Brown and Brand (20) measured the disequilibrium of the bc_1 complex in isolated mitochondria and found it to be ≈ 2 mV when the ATP synthase was inhibited with oligomycin whereas the kinetic model predicted a disequilibrium of 2.3 and 2.2 mV in HL-60 and RAW cells under oligomycin-inhibited conditions, respectively. These values are negligible. The disequilibrium increased to ≈ 48 mV when electron flux was stimulated with FCCP in the isolated mitochondria and the kinetic model predicted increases to 19

and 24 mV in HL-60 and RAW cells, respectively, when electron flux was stimulated with CCCP for the data in Fig. 3; the mitochondrial and cellular values are difficult to compare because the relative degree of uncoupling and electron flux in the two systems cannot be assessed. Although neither b_L and b_{H^+} , b_H and UQH_2/UQ , nor UQH_2/UQ and $\text{Cyt}c$ are strictly at equilibrium during the measurements due to the presence of a net flux, the analysis suggests that b_H and b_L are within 1 mV of equilibrium, b_H and UQ/UQH_2 are much less than 8 mV from equilibrium, and the disequilibrium between UQH_2/UQ and $\text{Cyt}c$ is corrected in large part by use of the kinetic model. Regardless of their disequilibrium during the measurements, the extrapolation to zero flux ensures that the proton stoichiometry is measured when all these couples are strictly at equilibrium and the oxidation state of the hemes does not depend on the absolute value of the rate constants in the model but only on the well-characterized midpoint potentials.

In the absence of pump slip (electron transfer without proton pumping) the net electron flux through complex I will be formally zero when complex I is at equilibrium ($\Delta G = 0$), and the pumping stoichiometry can be determined from the redox span and proton motive force. Unlike isolated mitochondria, the electron flux of mitochondria in cells cannot be fully inhibited while maintaining NADH/NAD^+ and UQH_2/UQ at intermediate oxidation states. The disequilibrium of complex I provides the driving force to generate a net flux so the approach employed was to reduce the flux to low values to minimize the disequilibrium of complex I, either with oligomycin to inhibit the ATP synthase or by culturing the cells overnight in glutamine-free media. The flux was then increased, either with the proton ionophore CCCP or by adding glutamine to the suspension medium, and then extrapolating $2\Delta E_s/\Delta P$ to values at zero flux (equilibrium) at which point it is equal to the proton pumping stoichiometry. The relationship between ΔG and flux is not necessarily linear, but the results presented here show that linearity is a good approximation over the range of fluxes studied and justifies the use of a linear force flux relationship in models of the electron transport chain (21). When this was carried out, it was found that the $\text{H}^+/2\text{e}^-$ stoichiometry was 4.4 ± 0.1 and 4.1 ± 0.1 for HL-60 and RAW cells, respectively, when flux was increased from the oligomycin-inhibited state with CCCP, and 4.0 ± 0.1 for RAW cells when flux was increased by adding glutamine to cells cultured overnight in the absence of glutamine. In no studies were values close to 3 found. These results are fully consistent with a proton pumping stoichiometry of $4\text{e}^-/2\text{H}^+$ when complex I operates in its authentic environment under physiological conditions (glutamine addition) and also at high proton motive force (oligomycin). This is in agreement with the analysis of the crystal structures, which has located a fourth putative proton pumping site close to the hydrophilic domain where electron transfer occurs (4, 22).

The greatest deviation from a stoichiometry of 4 was found in HL-60 cells and this may be due to the lower functional content of complex I in these cells compared with RAW cells. The relationship between flux and disequilibrium is not a unique function of ΔG but depends on how the disequilibrium is generated, e.g. the absolute values and relative changes in $\Delta\Psi$, ΔpH , and the redox potentials of the NADH/NAD^+ and UQH_2/UQ

pools. Even so, the 2-fold difference in gradient between flux and ΔG for HL-60 and RAW cells would suggest that the ratio of functional content of complex I and the functional content of the bc_1 complex is lower in HL-60 cells compared with RAW cells as a greater change in ΔG is needed to elicit the same change in bc_1 electron flux. This could either be the result of regulation of complex I through post translational modifications (23–25) or simply that the content of complex I is lower in HL-60 cells than RAW cells. In either case it would mean that the electron flux through complex I after inhibition with oligomycin was much higher in HL-60 cells compared with RAW cells, which would make the extrapolation to zero flux more error prone.

The reevaluation of the proton pumping stoichiometry from 4 to 3 (8) is partly based on the report by Hinkle *et al.* (7) that the redox span of complex I in state-4 is 360 mV and the report by Nicholls (26) that the proton motive force generated in state-4 is 220 mV giving a stoichiometry of $3.3\text{H}^+/2\text{e}^-$. However, Hinkle *et al.*, (7) used data from Muraoka and Slater (27) who reported that the measurements were carried out in a buffer containing 10 mM of inorganic phosphate. Nicholls (26) reports that ΔP is actually 178 mV under these conditions (Fig. 4 of Ref. 26) and not 220 mV, consistent with a stoichiometry of $4\text{H}^+/2\text{e}^-$, and emphasizes the need to measure all the parameters simultaneously. De Jong and Westerhoff (28) did measure all the parameters simultaneously, including redox potentials, $\Delta\Psi$, ΔpH , and matrix volume, and reported a stoichiometry of $3\text{H}^+/2\text{e}^-$ but were subsequently criticized for not including the non-specific binding of their $\Delta\Psi$ reporter by Brown and Brand (29) who measured the same parameters and obtained a stoichiometry of $4\text{H}^+/2\text{e}^-$ when correcting for the nonspecific binding and approaching equilibrium from both the forward and reverse direction.

Addition of oligomycin and CCCP are artificial methods of altering electron transport chain flux whereas addition of glutamine is a physiological method of changing flux. Glutamine enters the cell and activates mTOR (30–31), which is the master regulator of cell growth (32). Glutamine is also imported into the mitochondrial matrix where it is converted to glutamate by glutaminase and then the TCA cycle intermediate α -ketoglutarate by either glutamate dehydrogenase or aspartate transaminase (33). It is likely the increase in oxygen consumption is driven by the activation of growth secondary to mTOR rather than the increase in α -ketoglutarate because redox potential of the NADH pool did not become more reduced but rather oxidized by ≈ 11 mV from -347 ± 4 mV prior to addition of glutamine to -336 ± 5 mV 15 min after addition of glutamine. It is striking that complex I works closer to equilibrium and with a higher thermodynamic efficiency for a given flux under physiological conditions (\pm glutamine) compared with artificial conditions (oligomycin + CCCP). The observation that complex I does operate close to equilibrium puts strong limits on the proton pumping mechanism as equilibrium of the overall reaction requires equilibrium of all the partial reaction steps through which the enzyme passes during turnover. Some models of complex I proton pumping propose coupling of 4 protons in a single step (22). Pumping 4 protons at a physiological ΔP would require 720–800 mV of free energy,

Mammalian Complex I Pumps $4H^+ / 2e^-$

which is far above the thermal energy (26.7 mV), and represents a displacement from equilibrium of 12–13 orders of magnitude. It is difficult to imagine how such a step could be maintained close to equilibrium and emphasizes the need to validate a proton pumping scheme with a full kinetic model comprised of all the partial reactions (19, 34) operating in the presence of a physiological proton motive force, as we have done for the bc_1 complex.

REFERENCES

- Hirst, J. (2010) Towards the molecular mechanism of respiratory complex I. *Biochem. J.* **425**, 327–339
- Efremov, R. G., Baradaran, R., and Sazanov, L. A. (2010) The architecture of respiratory complex I. *Nature* **465**, 441–445
- Hunte, C., Zickermann, V., and Brandt, U. (2010) Functional modules and structural basis of conformational coupling in mitochondrial complex I. *Science* **329**, 448–451
- Efremov, R. G., and Sazanov, L. A. (2011) Structure of the membrane domain of respiratory complex I. *Nature* **476**, 414–420
- Efremov, R. G., and Sazanov, L. A. (2011) Respiratory complex I: 'steam engine' of the cell? *Curr. Opin. Struct. Biol.* **21**, 532–540
- Belevich, G., Knuuti, J., Verkhovskiy, M. I., Wikstrom, M., and Verkhovskaya, M. (2011) Probing the mechanistic role of the long α -helix in subunit L of respiratory Complex I from *Escherichia coli* by site-directed mutagenesis. *Mol. Microbiol.* **82**, 1086–1095
- Hinkle, P. C., Kumar, M. A., Resetar, A., and Harris, D. L. (1991) Mechanistic stoichiometry of mitochondrial oxidative phosphorylation. *Biochemistry* **30**, 3576–3582
- Wikström, M., and Hummer, G. (2012) Stoichiometry of proton translocation by respiratory complex I and its mechanistic implications. *Proc. Natl. Acad. Sci. U.S.A.* **109**, 4431–4436
- Villalobo, A., Alexandre, A., and Lehninger, A. L. (1984) H^+ stoichiometry of sites 1 + 2 of the respiratory chain of normal and tumor mitochondria. *Arch. Biochem. Biophys.* **233**, 417–427
- Costa, L. E., Reynafarje, B., and Lehninger, A. L. (1984) Stoichiometry of mitochondrial H^+ translocation coupled to succinate oxidation at level flow. *J. Biol. Chem.* **259**, 4802–4811
- Forman, N. G., and Wilson, D. F. (1982) Energetics and stoichiometry of oxidative phosphorylation from NADH to cytochrome c in isolated rat liver mitochondria. *J. Biol. Chem.* **257**, 12908–12915
- Watt, I. N., Montgomery, M. G., Runswick, M. J., Leslie, A. G., and Walker, J. E. (2010) Bioenergetic cost of making an adenosine triphosphate molecule in animal mitochondria. *Proc. Natl. Acad. Sci. U.S.A.* **107**, 16823–16827
- Kim, N., Ripple, M. O., and Springett, R. (2012) Measurement of the Mitochondrial Membrane Potential and pH Gradient from the Redox Poise of the Hemes of the bc_1 Complex. *Biophys. J.* **102**, 1194–1203
- Haller, T., Ortner, M., and Gnaiger, E. (1994) A respirometer for investigating oxidative cell metabolism: toward optimization of respiratory studies. *Anal. Biochem.* **218**, 338–342
- Kim, N., Ripple, M. O., and Springett, R. (2011) Spectral components of the alpha-band of cytochrome oxidase. *Biochim. Biophys. Acta* **1807**, 779–787
- Moser, C. C., Farid, T. A., Chobot, S. E., and Dutton, P. L. (2006) Electron tunneling chains of mitochondria. *Biochim. Biophys. Acta* **1757**, 1096–1109
- Shinkarev, V. P., Crofts, A. R., and Wraight, C. A. (2001) The electric field generated by photosynthetic reaction center induces rapid reversed electron transfer in the bc_1 complex. *Biochemistry* **40**, 12584–12590
- Gerencser, A. A., Chinopoulos, C., Birket, M. J., Jastroch, M., Vitelli, C., Nicholls, D. G., and Brand, M. D. (2012) Quantitative measurement of mitochondrial membrane potential in cultured cells: calcium-induced de- and hyperpolarization of neuronal mitochondria. *J. Physiol.* **590**, 2845–2871
- Ransac, S., Parisey, N., and Mazat, J. P. (2008) The loneliness of the electrons in the bc_1 complex. *Biochim. Biophys. Acta* **1777**, 1053–1059
- Brown, G. C., and Brand, M. D. (1985) Thermodynamic control of electron flux through mitochondrial cytochrome bc_1 complex. *Biochem. J.* **225**, 399–405
- Dzбек, J., and Korzeniewski, B. (2008) Control over the contribution of the mitochondrial membrane potential ($\Delta\psi$) and proton gradient (ΔpH) to the protonmotive force (Δp). *In silico* studies. *J. Biol. Chem.* **283**, 33232–33239
- Efremov, R. G., and Sazanov, L. A. (2012) The coupling mechanism of respiratory complex I - A structural and evolutionary perspective. *Biochim. Biophys. Acta* **1817**, 1785–1795
- Papa, S., Sardaneli, A. M., Scacco, S., Petruzzella, V., Technikova-Dobrova, Z., Vergari, R., and Signorile, A. (2002) The NADH: ubiquinone oxidoreductase (complex I) of the mammalian respiratory chain and the cAMP cascade. *J. Bioenerg. Biomembr.* **34**, 1–10
- Chen, R., Fearnley, I. M., Peak-Chew, S. Y., and Walker, J. E. (2004) The phosphorylation of subunits of complex I from bovine heart mitochondria. *J. Biol. Chem.* **279**, 26036–26045
- Schilling, B., Bharath, M. M. S., Row, R. H., Murray, J., Cusack, M. P., Capaldi, R. A., Freed, C. R., Prasad, K. N., Andersen, J. K., and Gibson, B. W. (2005) Rapid purification and mass spectrometric characterization of mitochondrial NADH dehydrogenase (Complex I) from rodent brain and a dopaminergic neuronal cell line. *Mol. Cell Proteomics* **4**, 84–96
- Nicholls, D. G. (1974) The influence of respiration and ATP hydrolysis on the proton-electrochemical gradient across the inner membrane of rat-liver mitochondria as determined by ion distribution. *Eur. J. Biochem.* **50**, 305–315
- Muraoka, S., and Slater, E. C. (1969) The redox states of respiratory-chain components in rat-liver mitochondria. II. The "crossover" on the transition from state 3 to state 4. *Biochim. Biophys. Acta* **180**, 227–236
- de Jonge, P. C., and Westerhoff, H. V. (1982) The proton-per-electron stoichiometry of 'site 1' of oxidative phosphorylation at high protonmotive force is close to 1.5. *Biochem. J.* **204**, 515–523
- Brown, G. C., and Brand, M. D. (1988) Proton/electron stoichiometry of mitochondrial complex I estimated from the equilibrium thermodynamic force ratio. *Biochem. J.* **252**, 473–479
- Wise, D. R., and Thompson, C. B. (2010) Glutamine addiction: a new therapeutic target in cancer. *Trends Biochem. Sci.* **35**, 427–433
- DeBerardinis, R. J., and Cheng, T. (2010) Q's next: the diverse functions of glutamine in metabolism, cell biology and cancer. *Oncogene* **29**, 313–324
- Shaw, R. J., and Cantley, L. C. (2006) Ras, PI(3)K and mTOR signalling controls tumour cell growth. *Nature* **441**, 424–430
- Moreadith, R. W., and Lehninger, A. L. (1984) The pathways of glutamate and glutamine oxidation by tumor cell mitochondria. Role of mitochondrial NAD(P) $^+$ -dependent malic enzyme. *J. Biol. Chem.* **259**, 6215–6221
- Ransac, S., Heiske, M., and Mazat, J. P. (2012) From *in silico* to *in spectro* kinetics of respiratory complex I. *Biochim. Biophys. Acta* **1817**, 1958–1969